



Inhibition of hydrogen and oxygen recombination using oxygen transfer reagent hemin chloride in Pt/TiO₂ dispersion for photocatalytic hydrogen generation

Zhen Li ^{a,b}, Bin Tian ^{a,b}, Wenlong Zhen ^a, Yuqi Wu ^a, Gongxuan Lu ^{a,*}

^a State Key Laboratory for Oxo Synthesis and Selective Oxidation Lanzhou Institute of Chemical Physics, Chinese Academy of Science, Lanzhou 730000, China

^b University of Chinese Academy of Science, Beijing 100049, China

ARTICLE INFO

Article history:

Received 23 June 2016

Received in revised form

20 September 2016

Accepted 18 October 2016

Available online 18 October 2016

Keywords:

Photocatalytic hydrogen generation

Inhibition of hydrogen and oxygen

recombination

Oxygen transfer reagent HC

Enhancement of hydrogen generation

Isotopes analysis

ABSTRACT

Recently, photocatalytic hydrogen generation from water-semiconductor catalyst dispersion attracted world-wide attention because the solar energy could be converted directly into hydrogen only in very simple set-up in scale-up scale. Although many photocatalysts were reported to be active for this reaction, the efficiency is still quite low. In this work, we found that hydrogen and oxygen recombination took place rapidly in the Pt/TiO₂ dispersion and resulted in very low hydrogen generation rate in pure water. The activation energy of H₂ and O₂ recombination reaction is 16.5 kJ/mol regardless of light irradiation or not. In this case, the photocatalytic evolved H₂ could react rapidly with the evolved O₂ to form H₂O again, eventually leading to no net H₂ and O₂ evolution during irradiation. The recombination of hydrogen and oxygen can be inhibited by addition of oxygen transfer reagent hemin chloride (HC). With help of HC, photocatalytic generated oxygen was captured by HC and transferred away from photocatalyst surface, then the backward reaction of hydrogen-oxygen recombination was successfully restrained. The photocatalytic hydrogen evolution amount in Pt/TiO₂ dispersion was significantly enhanced under this condition. The isotopes analysis results confirmed that both the H₂ and O₂ were from water. The HC could be recycled by releasing the O₂ with Ar gas bubbling. The HC could be poisoned by carbon monoxide and lost its oxygen transfer property, therefore no hydrogen could be formed under irradiation. This study clarified the main impediment reason of low efficient photocatalytic hydrogen generation in semiconductor-water dispersion and present available method to avoid this negative reaction. This finding will help to design high active catalytic system for solar energy to hydrogen conversion and open a new window for overall water splitting research.

© 2016 Elsevier B.V. All rights reserved.

1. Introduction

The photocatalytic overall water splitting could be realized by using photocatalytic electrodes with additional photovoltaic force (photoelectrolysis (PE)) or applying an electrolyzer driven by a solar cell (photovoltaic (PV) electrolysis) or light-irradiated suspended catalysts in water (photocatalysis (PC)) [1–3]. Although there are a large number of materials with suitable band gap potentials, there is very few material which function as a photocatalyst for over-

all water splitting. Most of the photocatalysts required sacrificial electron donor or acceptor addition for overall water splitting [4–7].

In the past decades, many efforts have been done to study overall water splitting in a wireless powder photocatalytic system to produce gaseous hydrogen and oxygen without any sacrificial reagent [8]. Using “Z-scheme” systems with two different semiconductors was a potential strategy to achieve stoichiometric cleavage of water by a two-photon excitation process [6,9], such as MgTa₂O_{6-x}N_y/TaON [10], SrTiO₃:Rh/BiVO₄ [11], and RuO₂–TaON/Pt–TaON [12] in the suspended mixture. Using iodine as a shuttle redox mediator has been also reported in a dispersed powder Z-scheme WO₃/SrTiO₃ system. [13] Another potential strategy was constructing different facets of semiconductor crystals, which could effectively separate the photogenerated electrons

* Corresponding author.

E-mail address: gxl@lzb.ac.cn (G. Lu).

and holes on the different facets for overall water splitting [14]. Selective loading redox cocatalysts on the different facets of a semiconductor crystal were reported [15]. The photocatalytic activities of those different facets semiconductor, such as TiO_2 [16], BiVO_4 [17], Cu_2WS_4 [18], Cu_2O [19], BiOCl [20], $\text{Sr}_2\text{Nb}_2\text{O}_7$ [21], BaTi_4O_7 [22], $\text{BaLa}_4\text{Ti}_4\text{O}_{15}$ [23], etc., can be dramatically improved due to the synergistic effect of facet charge separation and provision of redox active sites by cocatalysts spatially on the different facets [15]. Recently, using conjugated polymers (CPs) direct water splitting to form gaseous hydrogen and oxygen has been also achieved by the selective creation of both H_2 and O_2 cocatalysts on surface active sites of $\text{g-C}_3\text{N}_4$ [8].

However, photocatalytic water overall splitting still remains challenging because it is an uphill reaction. In generally, an electron acceptor such as the silver cations or an electron donor such as methanol are often added to the reaction solution to fulfill the photocatalytic generation of hydrogen or oxygen [24–28]. In the presence of sacrificial reagents, H_2 or O_2 could evolve, the undesirable backward reaction, water formation from H_2 and O_2 , can be strictly inhibited.

In fact, hydrogen and oxygen recombination is easily occurred over noble metal loaded catalysts at room temperature [29,30] and has been widely used in hydrogen removal passive autocatalytic recombiners (PAR) in water-cooled nuclear reactors under normal and emergency operating conditions [31–33]. This reaction can be inhibited in the presence of CO , CO_2 and H_2O (water vapor), and the catalysts are poisoned in this case.

Although hydrogen and oxygen recombination to water is well acknowledged, few publications have focused on its role on photocatalytic overall water splitting. Hydrogen and oxygen will co-exist in the liquid water in many cases. At 20 °C and 100 kPa, about 9.0 mg of oxygen can be dissolved in one liter of water, while only 1.63 mg of hydrogen can be dissolved in one liter of water at the same conditions. However, hydrogen and oxygen will form in a dispersion of semiconductor-water simultaneously theoretically under above band-gap irradiation. By this way, the harvesting and storing abundant solar energy in the cheap and clean chemical energy form of H_2 can be achieved. [34–36] Nevertheless, generated hydrogen and oxygen will co-exist in the same reaction media and the recombination of hydrogen and oxygen could not be avoided. Several strategies have been reported to inhibit this recombination, for example, the Pt with a higher oxidation state can be markedly inhibited the recombination of hydrogen and oxygen, while its hydrogen evolution capacity is still comparable to that of the benchmark of conventional metallic Pt cocatalyst. [37] Choi et al. reported that Cr_2O_3 barrier layer coated on Rh/SrTiO_3 could also suppress this back reaction. [38] However, those reports did not fully uncover the significant role of $\text{H}_2\text{-O}_2$ recombination on water splitting and fully inhibit this back-reaction. Inspired by biological system, we suppose HC can combine newly formed oxygen in the dispersion of semiconductor and decrease the oxygen concentration on the photocatalyst, then $\text{H}_2\text{-O}_2$ recombination can be suppressed.

In this work, the activation energy of H_2 and O_2 recombination reaction was measured, only about 16.5 kJ/mol, which implied the evolved H_2 could react rapidly with the evolved O_2 to form H_2O again, eventually leading to no net H_2 and O_2 in the reaction system. We utilize the oxygen transfer reagent HC to capture and transfer the evolved O_2 from water and then inhibit the backward recombination reaction of water splitting. By this strategy, the overall photocatalytic water splitting was enhanced. With help of HC, photocatalytic hydrogen evolution was significantly enhanced due to the inhibition of the recombination of hydrogen and oxygen. The HC could be recycled multi-cycles by releasing the O_2 with Ar gas bubbling and make photocatalytic activity for H_2 generation remained. The isotopes analysis results confirmed that both the H_2 and O_2 were generated from water. Poisoning HC by CO resulted in fully

loss of activity for hydrogen generation, H_2 evolution decreased immediately in this case. The possibility of HC act as a sacrificial reagent has been excluded.

2. Experimental section

2.1. Preparation of the Pt/P25 photocatalyst

The Pt/P25 photocatalyst was prepared by photoreduction method at room temperature in a sealed Pyrex flask (180 mL), which has a flat window (the efficient irradiation area is about 14 cm²). Typically, 1 g of P25 powder and 2.5 mL 5 mg/mL K_2PtCl_6 aqueous solution was added into 100 mL 10% (v/v) CH_3OH aqueous solution and then the mixture solution was ultrasonic treatment for 30 min. Prior to irradiation, the suspension was degassed by bubbling Ar gas for another 30 min. After reaction for 2 h under UV light irradiation, the resultant powder was collected by filtration, washing with ultrapure water and dried at room temperature and then redistributed into 1000 mL ultrapure water.

2.2. HC poisoned by CO

Typically, the 100 mg HC was dispersed in 100 mL H_2O with ultrasonic treatment in a sealed Pyrex flask (180 mL) and the suspension was degassed by bubbling Ar gas for 30 min. Then the HC was poisoned by bubbling CO gas for 60 min. The suspension was stirred on a magnetic stirrer at room temperature for 120 min. Finally, the resultant powder was collected by filtration, washed with ultrapure water and dried at room temperature.

2.3. Photocatalytic H_2 evolution activity

Photocatalytic experiments were performed at room temperature in a sealed Pyrex flask (180 mL), which has a flat window (the efficient irradiation area was about 14 cm²). In a typical reaction system, the 100 mL Pt/P25 suspended aqueous solution (the concentration of the dispersion of Pt/TiO₂ in water was 1 mg/mL) in the sealed Pyrex flask was degassed by bubbling Ar gas for 30 min and then using UV light irradiation to eliminate the remaining methanol until no H_2 evolved. After that, the 100 mg HC was added into 100 mL Pt/P25 (0.5 wt%) suspended aqueous solution and then the mixture solution was ultrasonic treatment for 30 min until the HC powder was uniformly dispersed. Prior to UV light irradiation, the suspension was degassed by bubbling Ar gas for another 30 min. The light source was a 250W medium pressure mercury vapor lamp. The amount of H_2 was measured using gas chromatography (Agilent 6820, TCD, 13× column, Ar carrier).

2.4. Isotopes tracer experiment

The isotopes tracer experiments have been performed in a sealed Pyrex reactor (180 mL). The pure D_2 was obtained via reaction of metal Na and D_2O mixture. The formed D_2 gas was firstly fed into a container filled with the calcium chloride anhydrous (about 1L) to adsorb the D_2O vapour. In order to make sure no D_2O vapour was mixed in the D_2 gas, we checked the MS signals before metallic Na was added in the D_2O solution by high pure Argon bubble, and no D_2O signal was observed in this step. As for the D_2 and O_2 combination experiment, we first replaced the reactor by high pure Argon gas, then the excess O_2 was injected in a sealed Pyrex reactor (180 mL) filled with dried Pt/P25 catalyst. The experiment proved the H_2 and O_2 come from water was also performed. Typically, 10 mg dry Pt/P25 and HC was dispersed in 10 mL D_2O or 10 mL H_2O^{18} in the sealed Pyrex flask. After ultrasonic treatment for 30 min, the suspended aqueous solution is degassed by bubbling Ar gas for another 30 min. After UV light irradiation for 4 h, the D_2

or O₂¹⁸ is evolved. The D₂O, D₂ and O₂¹⁸ were measured by GC-MS (MAT 271).

2.5. Working electrode preparation and photoelectrochemical measurements

Photocurrent responses of catalyst samples were measured on an electrochemical analyzer (CHI660E) in a homemade standard three-compartment cell, consisting of an organic glass enclosure with a quartz window and a 1.2 cm diameter opening opposite the window to the work electrode was clamped. The working electrodes were prepared by drop-coating sample suspensions directly onto the precleaned indium tin oxide glass (ITO glass) surface by microsyringe with an infrared heat lamp to speed drying. The surface of working electrode exposed to the electrolyte was a circular film with the geometrical surface areas of 1 cm². Platinum foil was used as a counter electrode and a saturated calomel electrode (SCE) was used as the reference electrode. The supporting electrolyte was 0.5 M H₂SO₄ aqueous solution. A 300-W Xe lamp was used for excitation light source. The unbiased anodic photocurrent was investigated with an amperometric current-time technique.

2.6. Characterizations

Transmission electron microscopy (TEM) images were taken with a Tecnai-G2-F30 field emission transmission electron microscope operating at accelerating voltage of 300 kV. The X-ray diffraction patterns (XRD) of the samples were recorded on a Rigaku B/Max-RB X-ray diffractometer with a nickel-filtrated Cu K α radiation. The accelerating voltage and current were 40 kV and 30 mA, respectively. XPS analysis was performed using a VG Scientific ESCALAB210-XPS photoelectron spectrometer with a Mg K α X-ray resource. UV-vis Diffuse Reflectance Spectra were obtained with a Shimadzu UV-3600 UV-vis-near-IR spectrophotometer. BaSO₄ was used as a reflectance standard. The fluorescence decay times were measured using the Horiba Jobin Yvon Data Station HUB operating in time-correlated single photon counting mode (TCSPC) with the time resolution of 200 ps. Nano LED diode emitting pulse sat 364 nm with 1 MHz repetition rate was used as an excitation source. Light-scattering Ludox solution was used to obtain the instrument response function (prompt). The time ranges are 0.055 ns/channel in 4096 effective channels. Horiba Jobin Yvon DAS6 fluorescence decay analysis software was used to fit the model functions to the experimental data.

3. Results and discussion

To achieve effective hydrogen evolution via photocatalytic overall water splitting, the H₂ and O₂ recombination reaction must be inhibited. [37,38] Unfortunately, H₂ and O₂ recombination back-reaction occurs very fast. As shown in Fig. 1, the injected stoichiometric H₂ and O₂ recombine rapidly over Pt/P25 photocatalyst in a sealed Pyrex flask. The detected H₂ decreased significantly in Fig. 1, indicating clear H₂ and O₂ recombination reaction. In order to confirm the product of H₂ and O₂ recombination, the isotopes tracer experiments were performed and the results were shown in Fig. 2. The O₂ and D₂ were injected into the reactor, after several minutes, the product was analyzed by GC-MS. The isotopes analysis results suggest the D₂ and O₂ recombination leads to D₂O formation. The m/z signal at 20.1 corresponds to the D₂O, while the m/z of 18.1, 28.1, 32.1 and 40.1 correspond to the trace amount of H₂O, nitrogen, oxygen and argon gas. In order to understand this recombination in detail, the kinetics of this recombination reaction were conducted at different temperatures, both under dark and light irradiation conditions. Base on the results in Fig. 3, the activation energy

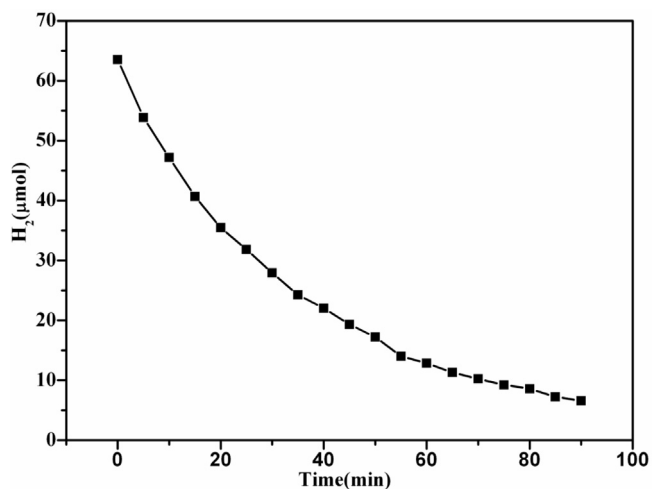


Fig. 1. The time courses of the H₂ and O₂ recombination reaction over Pt/P25 photocatalyst in a sealed Pyrex flask at room temperature.

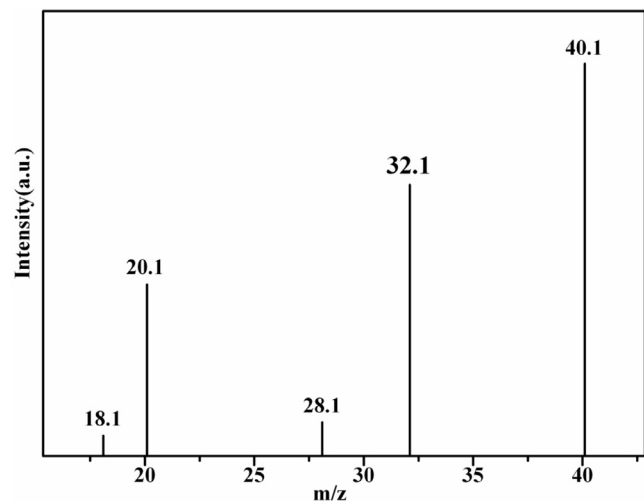


Fig. 2. GC-MS spectra obtained after injecting 0.5 mL samples of the gas phase species produced during H₂ and O₂ recombination reaction over Pt/P25 in a sealed Pyrex flask.

of thermal catalytic H₂-O₂ recombination reaction over Pt/P25 photocatalyst was calculated according to the Arrhenius equation. [39] It is about 16.5 kJ/mol, regardless of light irradiation or not. This result indicates the backward reaction of overall water splitting is a thermal catalytic process and the H₂ and O₂ can recombinant without too much extra energy barrier. Therefore, separating the generated H₂ and O₂ is one of the key and necessary factors to achieve the overall water splitting.

HC, an oxygen transfer reagent in the blood of animals, can effectively capture and transfer of O₂, and release O₂ when its pressure is low. We suppose the HC capture and transfer the O₂ generated from surface of photocatalyst in water, inhibit the backward reaction and promote the H₂ evolution. The time courses of H₂ evolution over Pt/P25 photocatalyst in pure water under UV light irradiation conditions were shown in Fig. 4a. As for the blank test, no H₂ was evolved over Pt/P25 photocatalyst in pure water under UV light irradiation. That might due to the rapid backward reaction of overall water splitting. When HC was added, the H₂ generation was achieved and the amount of H₂ was 25.9 μmol in 4 h. This result implies the HC can effectively capture the evolved O₂ from catalyst surface and transfer it away from its formation site over catalyst during overall water splitting, and inhibit the generated H₂ and

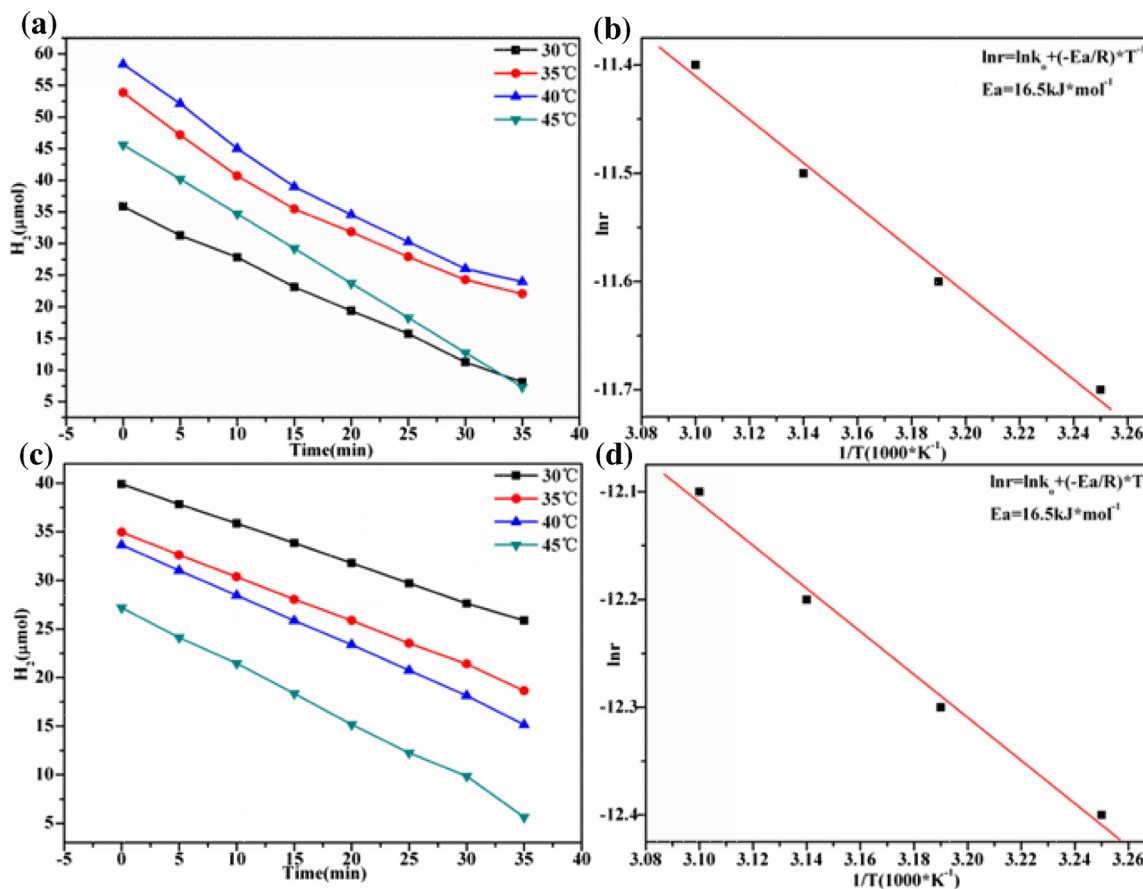


Fig. 3. Hydrogen recombination reaction kinetics curves over Pt/P25 photocatalyst in a sealed Pyrex flask with injecting stoichiometric H_2 and O_2 (a,c) and Arrhenius plot for determination of the activation energy (b,d). (a and b were in the dark, c and d were in the UV light irradiation).

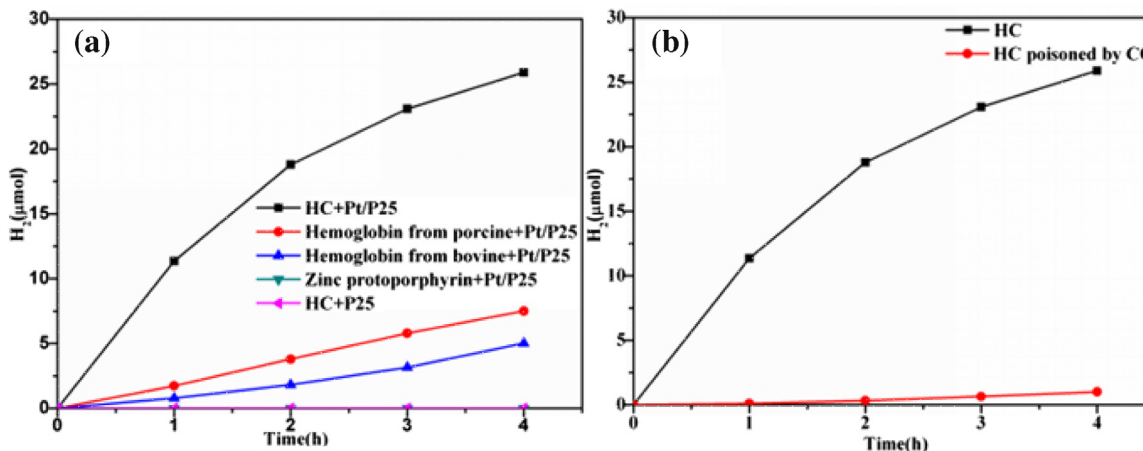


Fig. 4. The time courses of H_2 evolution over Pt/P25 or P25 photocatalyst in pure water under UV light irradiation conditions with adding 100 mg HC, hemoglobin from porcine and bovine and Zinc protoporphyrin (a), the time courses of H_2 evolution over Pt/P25 with 100 mg HC and poisoned HC by CO (b).

O_2 recombination. For comparison, hemoglobin (with similar function of transfer oxygen to hemin chloride) was added in the Pt/P25 suspended aqueous solution, and the photocatalytic H_2 generation was also achieved. There are 7.5 and 5.3 μmol H_2 evolved in the hemoglobin system from porcine and bovine, respectively. Those results indicated that overall photocatalytic water splitting can be achieved if the newly formed oxygen is removed from semiconductor catalyst surface and the $\text{H}_2\text{-O}_2$ recombination back-reaction is inhibited. In order to prove the HC capture the O_2 rather than as a sacrifice reagent for H_2 evolution, the Zinc protoporphyrin was

added into reaction system separately. The structure of Zinc protoporphyrin is similar to the HC, except for the central metal atoms. But the Zinc protoporphyrin could not transfer the O_2 in the blood of animals. In this case, only a trace amount of H_2 evolved over Pt/P25 photocatalyst. This result suggests that the HC can capture the O_2 rather than as a sacrifice reagent for H_2 evolution. In addition, the time courses of H_2 evolution over P25 photocatalyst in HC system indicated that no H_2 was detected in the absence of Pt. This result implies the Pt acts as the reaction active site for the H_2 evolution. The experiment of HC poisoned by CO for H_2 evolution

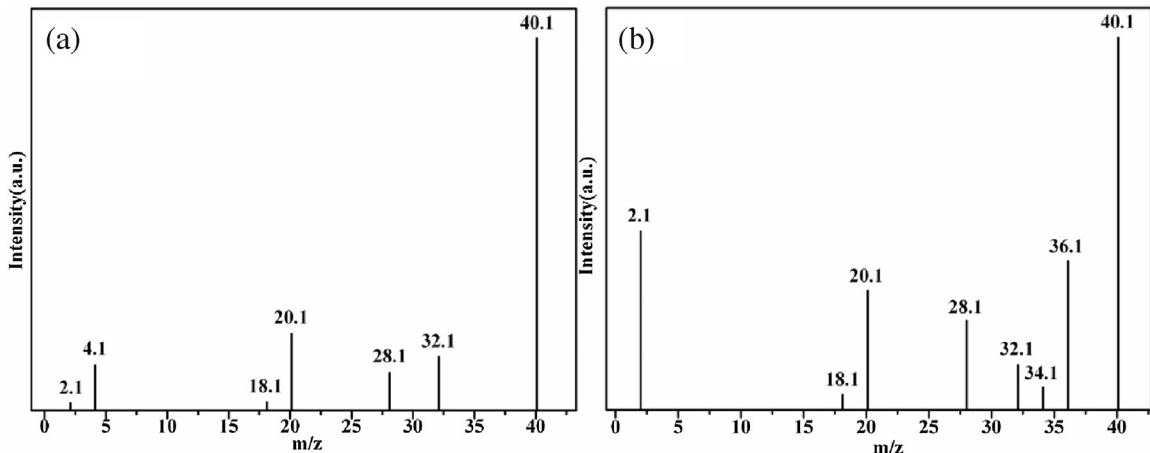


Fig. 5. GC-MS spectra obtained after injecting 0.5 mL samples of the gas phase species produced by D_2O (a) and H_2O^{18} (b) splitting over Pt/P25 in a sealed Pyrex flask during UV light irradiation 4 h.

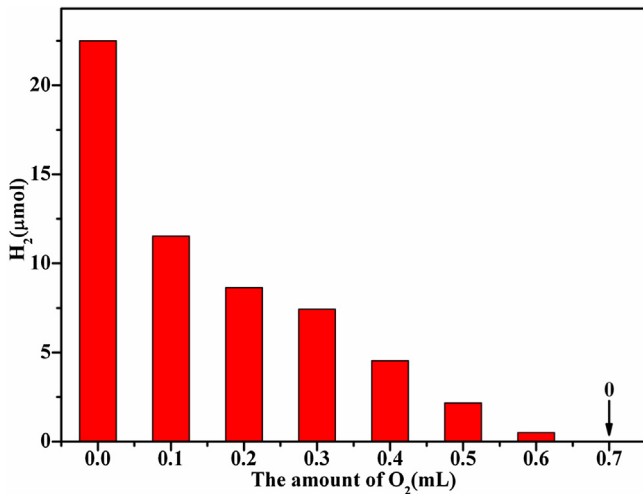


Fig. 6. The effect of the amount of injected O_2 on the H_2 evolution activity over Pt/P25 photocatalysts under UV light irradiation.

was also performed to further exclude the HC act as a sacrificial reagent. The result in Fig. 4b showed that the activity of H_2 evolution was dropped immediately when HC was poisoned, due to the irreversible combination between CO and HC, which lead to the function failure of HC capture to O_2 .

In order to firmly identify H_2 and O_2 generated via water splitting, more isotopic tracer experiments were carried out and the results were shown in Fig. 5. In Fig. 5a, the D_2O was used to prove the D_2 from water. The isotopes analysis results showed both D_2 and H_2 were detected. It indicates the D_2 comes from water splitting. In Fig. 5b, the H_2O^{18} was used to prove the O_2 from water. The isotopes analysis results showed that O_2^{18} , $\text{O}^{16}\text{O}^{18}$ and O_2 were all detected, indicating the O_2 also from water splitting. These results prove the H_2 and O_2 come from overall photocatalytic water splitting, and the HC here acts as O_2 transfer reagent rather than sacrificing reagent. The effect of the amount of injected O_2 on the H_2 evolution activity over Pt/P25 photocatalyst was also performed under UV light irradiation to further prove the O_2 capture function of HC, and the result was shown in Fig. 6. The activity of H_2 evolution over Pt/P25 photocatalyst was decreased gradually when the amount of injected O_2 increased from 0 to 0.7 mL. When 0.7 mL O_2 was injected into the system, no H_2 was detected. This result suggests that no hydrogen was generated when the O_2 capture ability of HC reached saturation.

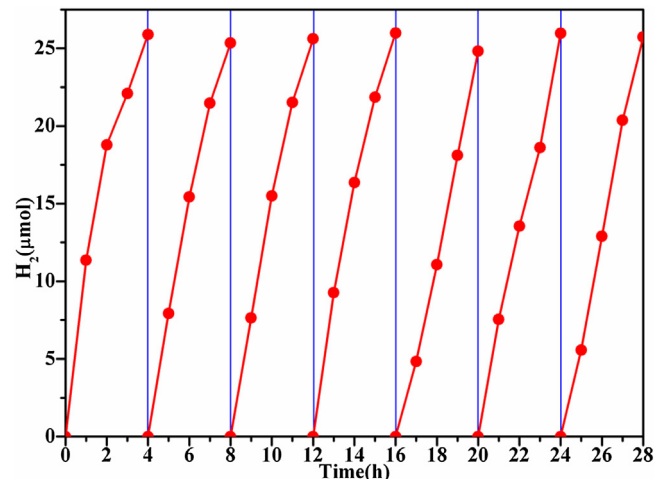


Fig. 7. The oxygen transfer regent regenerate and the stability of H_2 evolution over Pt/P25 photocatalyst under UV light irradiation. The reaction was continued for 28 h. After every run, the reaction system was bubbled by Ar gas.

tion. However, the HC ability of capturing O_2 can regenerate by bubbling Ar gas to release the O_2 (shown in Fig. 7). After each run, the reaction system was bubbled by Ar gas to release the O_2 to regenerate the oxygen transfer reagent. In this case, the photocatalysts gave stable recycle activity for hydrogen generation, and no obvious deactivation was observed after 28 h of reaction.

The XRD patterns of HC, P25, Pt/P25, HC/Pt/P25 before reaction and HC/Pt/P25 after reaction photocatalysts were carried out and the results were shown in Fig. 8. For the Pt/P25 photocatalyst, the series peaks were belonged to the typical diffraction peaks of P25. [40] After loading Pt nanoparticles on the surface of P25 by *in situ* photoreduction, the obvious diffraction peak at 18.1° was attributed to the (111) facet of Pt nanoparticles (JPCDS#01-1194). However, no obvious differences of the XRD diffraction of HC/Pt/P25 before and after reaction could be detected. This result implied the HC was stable in the process of the reaction and it also further proves the HC acted as oxygen transfer reagent rather than sacrificing reagent. This point was also supported by the UV-vis absorption spectra of HC, P25, Pt/P25, HC/Pt/P25 before and after reaction (shown in Fig. 9). There is no obvious change of absorption peaks of HC/Pt/P25 before and after reaction.

The XPS spectra of HC, P25, Pt/P25, HC/Pt/P25 before and after reaction were measured and the results were shown in Fig. 10.

Table 1

Fluorescence lifetime measurements of P25, Pt/P25, HC/Pt/P25 photocatalysts.

P25 systems	Lifetime, $\langle \tau \rangle$ (ns)	Pre-exponential factors B	Average lifetime, $\langle \tau \rangle$ (ns)	χ^2
P25	2.09	$B_1 = 1$	2.09	1.102
Pt/P25	$\tau_1 = 1.02$ $\tau_2 = 4.07$	$B_1 = 0.0269$ $B_2 = 0.9731$	3.99	1.301
HC + Pt/P25	$\tau_1 = 4.03$ $\tau_2 = 6.67$	$B_1 = 0.0248$ $B_2 = 0.9752$	6.60	1.295

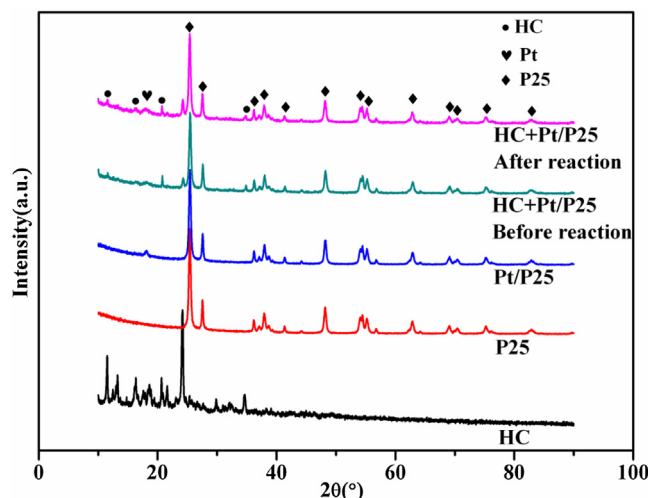


Fig. 8. XRD patterns of HC, P25, Pt/P25, HC/Pt/P25 before and after reaction.

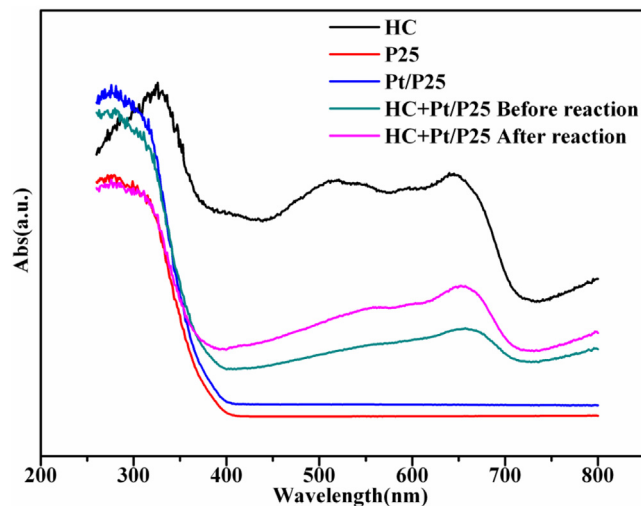


Fig. 9. The UV-vis absorption spectra of HC, P25, Pt/P25, HC/Pt/P25 before and after reaction.

In Fig. 10a, the binding energy of 458.7 and 464.5 eV corresponds to $Ti\ 2p_{3/2}$ and $2p_{1/2}$, respectively. After loading Pt nanoparticles on the surface of P25, the binding energy of P25 $2p_{3/2}$ shifts from 458.7 to 458.8 eV. This result suggests the electron transfer tendency from Ti to Pt, [41] which implies the Pt can enhance the charge carrier separation. Adding HC in the reaction system, the binding energy of $Ti\ 2p_{3/2}$ changes more positive, which indicates the HC has an interaction with the P25. In Fig. 10b, the binding energy of 71.1 and 74.5 eV corresponds to $Pt\ 4f_{7/2}$ and $4f_{5/2}$, respectively. No obvious differences are detected after adding the HC. In Fig. 10c, in the HC and HC/Pt/P25 before reaction systems, the Fe species shows same chemical state. However, the binding energy of $Fe\ 2p_{3/2}$ shifted from 711.2 to 711.7 eV after reaction. This result indicates the HC have captured the O_2 generated from overall water splitting in the UV light irradiation. The fluorescence lifetime measurements of P25, Pt/P25, HC/Pt/P25 photocatalysts were carried out and results were shown in Table 1. The average fluorescence lifetime of P25 is 2.09 ns. After loading Pt nanoparticles on the surface of P25, the average fluorescence lifetime increased to 3.99 ns. These results suggest that there is interaction between P25 and Pt nanoparticles, which can effectively enhance the separation of charge carriers [42–46]. Addition of HC further increased the average fluorescence lifetime to 6.60 ns. Combined with the results of XPS, longer lifetime reflects capture the O_2 generated from overall water splitting further enhance the charge carriers separation.

To study the structure and morphology of Pt/P25 photocatalyst, transmission electron microscopy (TEM) images were tested and the results were shown in Fig. 11. The high-resolution TEM (HRTEM) of Pt/P25 photocatalyst was shown in Fig. 11a. The lattice spacing of 0.23 nm could be assigned to the (111) facet of Pt nanoparticles and the lattice spacing of 0.17 nm could be assigned to the (211) facet of P25. In Fig. 11b, the photocatalyst showed the typical morphology and structure of P25 and the Pt nanoparticles were uniformly distributed on the surface of P25. Fig. 11c clearly showed that the distribution of Ti, O and Pt elements were relatively homogeneous in Pt/P25 photocatalyst, which also proved that the Pt nanoparticles were uniformly dispersed on the surface of P25.

Photoelectrochemical experiments were performed to study the photoinduced electron transfer processes. As shown in Fig. 12, the response to UV light could be seen during on-off cycles of visible light irradiation, while the Pt/P25/ITO electrode produced a

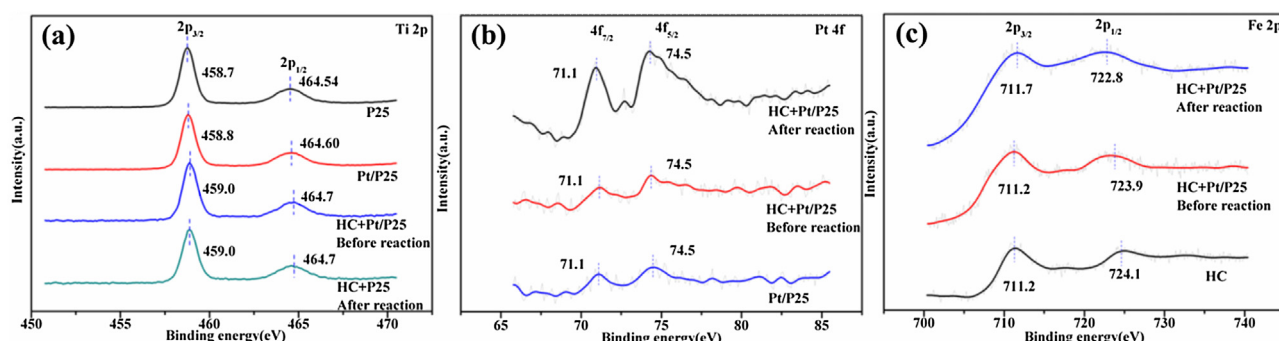


Fig. 10. The XPS spectra of HC, P25, Pt/P25, HC/Pt/P25 before and after reaction.

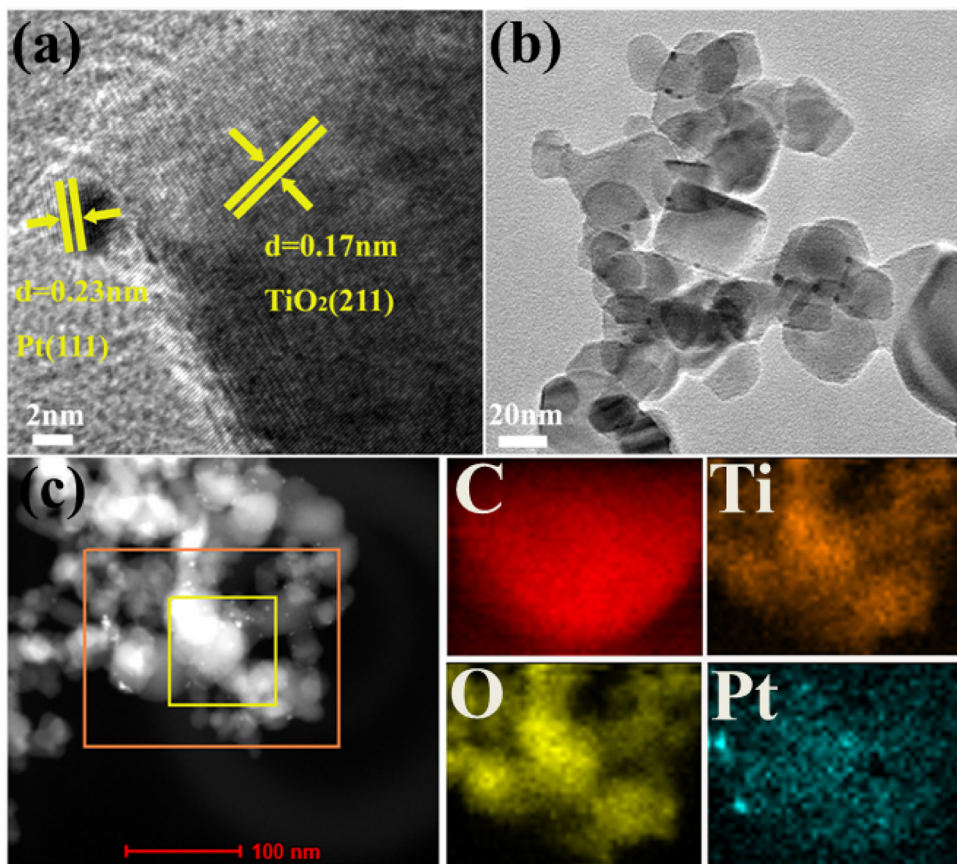


Fig. 11. The HRTEM images of Pt/P25 photocatalyst (a); TEM images of Pt/P25 photocatalyst (b); HAADF-STEM (high-angle annular dark field scanning transmission electron microscopy) image and elemental mapping images of Pt/P25 photocatalyst (c).

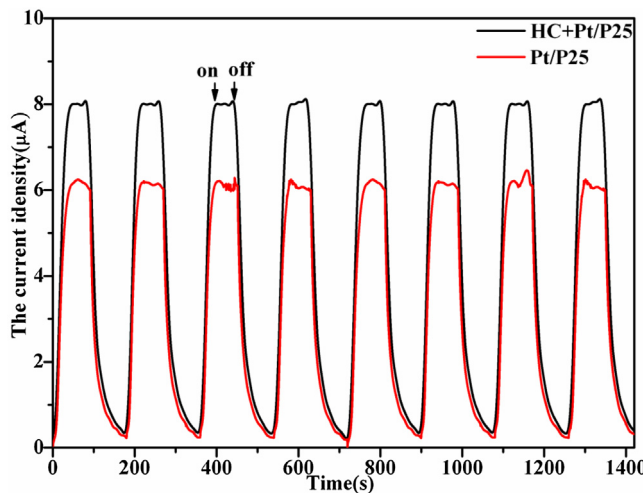


Fig. 12. Transient photocurrent time profiles of Pt/P25 and HC/Pt/P25 photocatalysts on ITO glass in 0.5 M H₂SO₄ aqueous solution under UV light irradiation.

low photocurrent about 6.2 μ A. The observed unbiased transient photocurrent with HC/Pt/P25/ITO electrode was promoted under similar experimental conditions to about 8.0 μ A. Results indicated that HC capture of the O₂ generated from overall water splitting further enhanced the charge carriers separation and H₂ evolution activity. Voltammetric profiles of Pt/P25 and HC/Pt/P25 photocatalysts on ITO glass in 0.5 M H₂SO₄ aqueous solution were also performed (shown in Fig. 13). For the Pt/P25/ITO electrode, the peak centered at -0.05 V could be easily observed, which corresponded

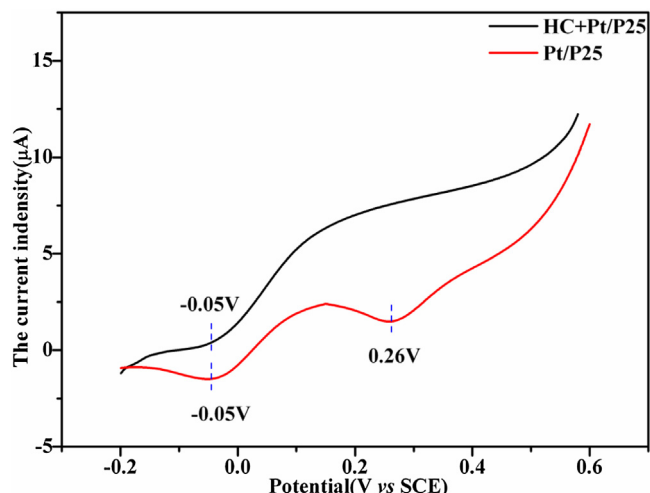
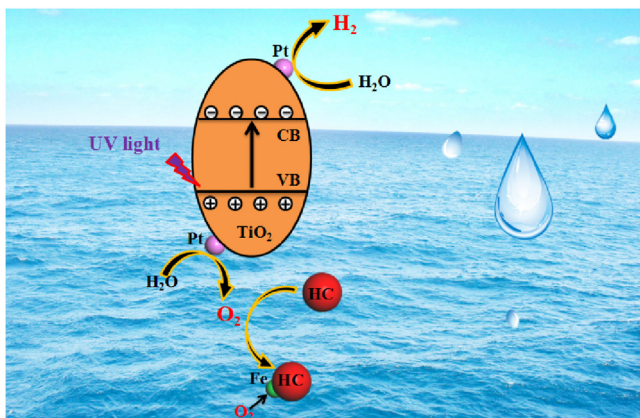


Fig. 13. Voltammetric profiles of Pt/P25 and HC/Pt/P25 photocatalysts on ITO glass in 0.5 M H₂SO₄ aqueous solution under N₂ bubbling condition. Sweep rate: 50 mV/s.

to desorption of H₂ and the peak centered at 0.26 V was attributed to desorption of O₂. However, for the HC/Pt/P25/ITO electrode, the peak centered at 0.26 V was disappeared due to the O₂ captured by the HC.

The whole reaction process of photocatalysis overall water splitting over the HC/Pt/P25 can be explained in terms of Scheme 1. The semiconductor P25 absorbs UV light to excite the electrons from the valence band to the conduction band. The charge carriers transfer to the surface of the P25 semiconductor. With the Pt nanoparticles



Scheme 1. The proposed reaction mechanism of overall water splitting over HC/Pt/TiO₂ photocatalyst under UV light irradiation.

as the active sites, the electrons reduce H⁺ to form H₂, while the holes oxidize the H₂O to form oxygen. The generated H₂ and O₂ will recombinant rapidly to form water if there is no HC on the catalyst surface. The HC can capture and transfer the newly generated O₂ and inhibit the H₂-O₂ recombination backward reaction, leading to the continuous H₂ evolution.

4. Conclusion

In this work, the overall photocatalytic water splitting was achieved by using the HC for capturing and transfer of newly generated O₂, which can effectively inhibit the generated H₂ and O₂ recombination. As a result, the H₂ evolution was significantly enhanced. The HC could be recycled by releasing the O₂ with Ar gas bubbling. The isotopes tracer tests, poisoning HC by CO gas and zinc protoporphyrin as reference experiments indicated that the generated H₂ and O₂ came from water and the HC acted as oxygen transfer reagent rather than sacrificial reagent. This study clarified the main impediment reason of low efficient photocatalytic hydrogen generation in semiconductor-water dispersion and present available method to avoid this negative reaction. This finding will help to design high active catalytic system for solar energy to hydrogen conversion and open a new window for overall water splitting research.

Acknowledgment

This work is supported by the NSF of China (grant no. 21673262 and 21433007), respectively.

References

- [1] M. Graetzel, Acc. Chem. Res. 14 (1981) 376–384.
- [2] C.K. Gratzel, M. Gratzel, J. Am. Chem. Soc. 101 (1979) 7741–7743.
- [3] A. Fujishima, K. Honda, K. Kohayakawa, Nature 238 (1972) 37–38.
- [4] L. Ma, X. Kang, S. Hu, F. Wang, J. Mol. Catal. (China) 29 (2015) 359–368.
- [5] N. Srinivasan, Y. Shiga, D. Atarashi, E. Sakai, M. Miyauchi, Appl. Catal. B 179 (2015) 113–121.
- [6] N. Srinivasan, E. Sakai, M. Miyauchi, ACS Catal. 6 (2016) 2197–2200.
- [7] S. Peng, M. Ding, T. Yi, Y. Li, J. Mol. Catal. (China) 28 (2014) 466–473.
- [8] G.G. Zhang, Z.A. Lan, L.H. Lin, S. Lin, X.C. Wang, Chem. Sci. 7 (2016) 3062–3066.
- [9] K. Maeda, ACS Catal. 3 (2013) 1486–1503.
- [10] S.C. Chen, Y. Qi, T. Hisatomi, Q. Ding, T. Asai, Z. Li, S.S. Ma, K.F.X. Zhang, K. Domen, C. Li, Angew. Chem. Int. Ed. 54 (2015) 8498–8501.
- [11] A. Iwase, Y.H. Ng, Y. Ishiguro, A. Kudo, R. Amal, J. Am. Chem. Soc. 133 (2011) 11054–11057.
- [12] K. Maeda, R. Abe, K. Domen, J. Phys. Chem. C 115 (2011) 3057–3064.
- [13] K. Sayama, K. Mukasa, R. Abe, Y. Abe, H. Arakawa, Chem. Commun. (2001) 2416–2417.
- [14] Q. Zhang, Z. Li, S.Y. Wang, R.G. Li, X.W. Zhang, Z.X. Liang, H.X. Han, S.J. Liao, C. Li, ACS Catal. 6 (2016) 2182–2191.
- [15] R.G. Li, H.X. Han, F.X. Zhang, D. Wang, C. Li, Energy Environ. Sci. 7 (2014) 1369–1376.
- [16] J. Pan, G. Liu, G.Q. Lu, H.M. Cheng, Angew. Chem. Int. Ed. 50 (2011) 2133–2137.
- [17] R.G. Li, F.X. Zhang, D. Wang, J.X. Yang, M.R. Li, J. Zhu, X. Zhou, H.X. Han, C. Li, Nat. Commun. 4 (2013) 1432–1438.
- [18] N.X. Li, M.C. Liu, Z.H. Zhou, J.C. Zhou, Y.M. Sun, L.J. Guo, Nanoscale 6 (2014) 9695–9702.
- [19] L.Z. Zhang, J.W. Shi, M.C. Liu, D.W. Jing, L.J. Guo, Chem. Commun. 50 (2014) 192–194.
- [20] K. Jiang, K. Zhao, X.Y. Xiao, L.Z. Zhang, J. Am. Chem. Soc. 134 (2012) 4473–4476.
- [21] A. Kudo, H. Kato, S. Nakagawa, J. Phys. Chem. B 104 (2000) 571–575.
- [22] M. Kohno, S. Ogura, K. Sato, Y. Inoue, Chem. Phys. Lett. 267 (1997) 72–76.
- [23] K. Iizuka, T. Wato, Y. Misaki, K. Saito, A. Kudo, J. Am. Chem. Soc. 133 (2011) 20863–20868.
- [24] K. Maeda, K. Domen, J. Phys. Chem. C 111 (2007) 7851–7861.
- [25] G. Iervolino, V. Vaiano, J.J. Murcia, L. Rizzo, G. Ventre, G. Pepe, P. Campiglia, M.C. Hidalgo, J.A. Navio, D. Sannino, J. Catal. 339 (2016) 47–56.
- [26] V. Vaiano, G. Iervolino, G. Sarno, D. Sannino, L. Rizzo, J.J.M. Mesa, M.C. Hidalgo, J.A. Navio, Oil Gas Sci. Technol.-Revue d'IFP Energies Nouvelles 70 (2015) 891–902.
- [27] A.M.D. Fornaria, M.B.D. Araujoa, C.B. Duarte, G. Machadob, S.R. Teixeirac, D.E. Weibela, Int. J. Hydrogen Energy 41 (2016) 11599–11607.
- [28] F.J. López-Tenllado, J. Hidalgo-Carrillo, V. Montes, A. Marinas, F.J. Urbano, J.M. Marinas, L. Ilieva, T. Tabakova, F. Reid, Catal. Today, doi.org/10.1016/j.cattod.2016.05.009.
- [29] E. Lalik, A. Drelinkiewicz, R. Kosydar, R. Tokarz-Sobieraj, M. Witko, T. Szumelka, J. Gurgul, D. Duraczynska, Appl. Catal. A 517 (2016) 196–210.
- [30] E. Lalik, A. Drelinkiewicz, R. Kosydar, W. Rojek, T. Machej, J. Gurgul, T. Szumelka, M. Kołodziej, E. Bielanska, Int. J. Hydrogen Energy 40 (2015) 16127–16136.
- [31] A.D. He, M.L. Ye, Z.H. Tang, S.J. Lu, Y.Z. Gu, X.G. Fan, L. Zhao, J.B. Gao, Nucl. Chem. 230 (1998) 253–255.
- [32] S. Roginskij, A. Sechter, 2 (1934) 310–312.
- [33] L. Farkas, H. Sachsse, Zeitschrift Fur Physikalische Chemie-Abteilung B-Chemie Der Elementarprozesse Aufbau Der Materie 27 (1934) 111–129.
- [34] T. Hisatomi, J. Kubota, K. Domen, Chem. Soc. Rev. 43 (2014) 7520–7535.
- [35] X. Chen, S. Shen, L. Guo, S.S. Mao, Chem. Rev. 110 (2010) 6503–6570.
- [36] A. Kudo, Y. Misaki, Chem. Soc. Rev. 38 (2009) 253–278.
- [37] Y.H. Li, J. Xing, Z.J. Chen, Z. Li, F. Tian, L.R. Zheng, H.F. Wang, P. Hu, H.J. Zhao, H.G. Yang, Nat. Commun. 4 (2013) 2500.
- [38] Y.J. Cho, G.H. Moon, T. Kanazawa, K. Maeda, W. Choi, Chem. Commun. 52 (2016) 9636–9639.
- [39] Y.P. Guo, Q.H. Feng, Z.P. Dong, J.T. Ma, J. Mol. Catal. A: Chem. 378 (2013) 273–278.
- [40] E.T. Cui, G.X. Lu, Int. J. Hydrogen Energy 39 (2014) 8959–8968.
- [41] Z. Li, C. Kong, G.X. Lu, Int. J. Hydrogen Energy 40 (2015) 9061–9068.
- [42] Z. Li, Q.S. Wang, C. Kong, Y.Q. Wu, Y.X. Li, G.X. Lu, J. Phys. Chem. C 119 (2015) 13561–13568.
- [43] Z. Li, C. Kong, G.X. Lu, J. Phys. Chem. C 120 (2016) 56–63.
- [44] W.L. Zhen, J.T. Ma, G.X. Lu, Appl. Catal. B 190 (2016) 12–25.
- [45] Z. Li, Y.Q. Wu, G.X. Lu, Appl. Catal. B 188 (2016) 56–64.
- [46] B. Tian, Z. Li, W.L. Zhen, G.X. Lu, J. Phys. Chem. C 120 (2016) 6409–6415.